

Mechanism of Codeposition of Silicon Carbide with Electrolytic Cobalt

Bing Joe Hwang and Cheng Sheng Hwang

Department of Chemical Engineering, National Taiwan Institute of Technology, Taipei, Taiwan 106, China

ABSTRACT

The mechanism of codeposition of silicon carbide with electrolytic cobalt was studied. A theoretical model of codeposition is developed here which provides a more complete insight to the mechanism of electrolytic codeposition than Guglielmi's model. The model gives a more general expression relating weight percent of embedded particles to current density for different suspension particle concentration for the Co-SiC codeposition system which cannot be described by Guglielmi's model.

Interest in electrodeposited composite coatings has increased rapidly¹⁻⁶ due to their expected new engineering applications.⁵ Such coatings are produced by codeposition of fine inert particles in a metal matrix from electrolytic or electroless baths. For example, a cobalt coating in conjunction with silicon carbide particles was developed and has been proven highly successful.

Although the technique has been developed considerably from the practical point of view, the theoretical details on the codeposition mechanism are not well understood. Three mechanisms, namely, mechanical inclusion, electrophoresis, and adsorption of inert particles onto the cathode, have been proposed to explain the observed codeposition. The relative importance of these three processes cannot be deduced from published experimental work as some results are contradictory. Guglielmi⁷ has proposed a mathematical model for the electrodeposition of inert particles which is based on two successive adsorption steps. In the first step a loose adsorption which has an essentially physical character results in a high degree of coverage of cathode by particles which are in equilibrium with the particles in suspension solution. The particles are still surrounded by adsorbed ions and solvent molecules. In the second step this screen is broken through so that a strong electrochemical adsorption of the particles on the cathode takes place, namely, strong adsorption. The inert particles are now permanently bound to the cathode and consequently are embedded in the deposit. The formula so deduced is

$$\frac{C_p}{\alpha} = \frac{W_i i_0}{n F d v_0} \cdot \exp(A - B)\eta \cdot (1/K + C_p) \quad [1]$$

where C_p is the concentration of suspended particles, α is the volume fraction of particles in the deposit, F , W , and d are the Faraday constant, atomic weight, and density of the electrodeposited metal, respectively. The parameters i_0 and A are related to the metal deposition and are the constants in the Tafel equation. Similarly, the parameters v_0 and B are related to the inert particle deposition. K is derived from the Langmuir adsorption isotherm and depends essentially on the intensity of the interaction between particles and cathode. The validity of this model has been verified for different codeposition systems such as SiC and TiO₂ with nickel from sulfamate baths,⁷ α -Al₂O₃ with copper from acid copper sulfate baths,⁸ Al₂O₃ with nickel from Watts bath,⁹ and TiO₂ with copper from acidic copper sulfate baths.¹⁰ However, some codeposition systems question the generality of the model, such as α -Al₂O₃ with copper from acid copper sulfate baths¹ and Al₂O₃ with gold from cyanide baths.¹ Guglielmi's model cannot describe the weight percent of the particles in the deposit and the current density relationship shown in Fig. 1. A more general model for the codeposition system must be developed.

Foster and Kariapper¹¹ have proposed a mathematical expression that could describe the effect of hydrodynamics. Celis *et al.*¹² have proposed a mathematical model from a statistical approach of the incorporation of particles. Because of the complex interrelationship between some of

these factors (transition current density, limiting current density, amount of ions adsorbed on particles, diffusion layer thickness, interaction parameter between free and adsorbed ions due to current density effect, etc.), a limited amount of work was done to prove the validity of these two models.

A more general model is proposed here to describe the mechanism of the electrolytic codeposition process and it is verified by experimental results of a silicon carbide-electrolytic cobalt system.

Experimental

Abrasive grade silicon carbide powders (Yakuri chemicals, α -SiC) of 3 μ m were used for the investigation. The powders were thoroughly cleaned in an acetone solvent, and treated with hot dilute nitric acid to remove any organic impurities, washed thoroughly in distilled water, and dried. All chemicals were of reagent grade and used without further purification. A cobalt sulfate bath was prepared by dissolving 100 g/dm³ CoSO₄ · 7H₂O, 15 g/dm³ CoCl₂ · 6H₂O, 10 g/dm³ KCl, and 25 g/dm³ H₃BO₃ in distilled water. The plating experiments were conducted in an acrylic reactor with two baffles (Fig. 2). The vertical brass cathodes were placed on the center of the designed reactor so that a good uniformity of the deposits could be obtained. The uniformity of current density in the designed reactor was checked from the distribution of deposited particles by the optical microscopy. The results indicate that a good uniformity is obtained in the designed reactor. The concentration of silicon carbide powder used in suspension in the electrolyte was varied from 2-10 g/dm³. The bath was operated at 30 ± 1°C, the current density employed was in the range 0.1 to 6 A/dm², pH was controlled at 4 and the total number of coulombs supplied was 810 C per batch. Sheets of electrolytic cobalt served as anodes while brass served as cathodes. The electrodes were pretreated in the usual way.

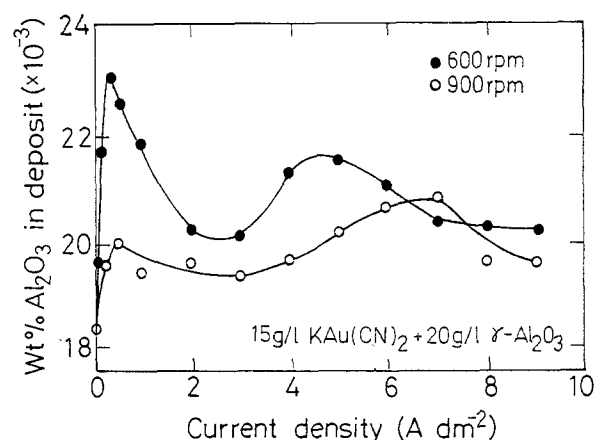


Fig. 1. Weight percent of particles on deposit against current density at different rotation speeds.¹

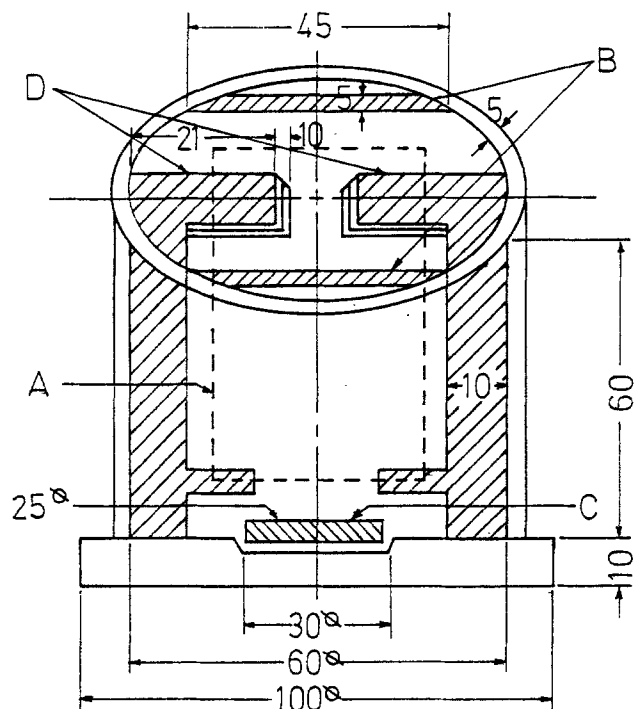


Fig. 2. Details of the electrolytic reactor; (A) cathode; (B) anodes; (C) magnetic stirrer; and (D) baffles.

A power supply served as the direct current source. The bath was agitated with a magnetically driven Teflon-coated stirring bar. The mixing rate was controlled at 400 rpm. The total weight of the deposits was determined by microbalance. The weight percent of silicon carbide in the deposits was analyzed by x-ray fluorescent spectrometry. Before this measurement, the prepared standards and deposits were ground and polished with 1 μm diamond suspension at 150 rpm and 100 N for 20 s (Struers, Abramin).

Theoretical Model

Model description.—As shown in Fig. 3, an adsorbed layer of ionic species is created around the inert particles while the particles are added to the plating solution.¹² On its way from the bulk solution to deposit the inert particle must proceed through three stages; (i) the particles are transferred primarily by forced convection; (ii) the particles with their adsorbed ionic cloud are adsorbed loosely at

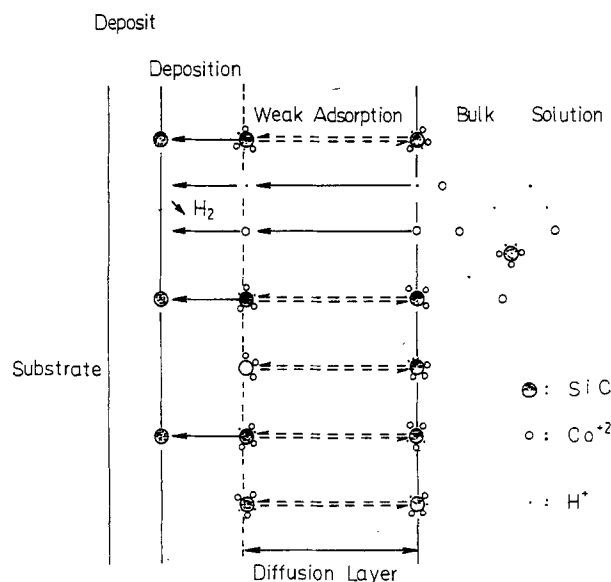


Fig. 3. Reaction sequence of codeposition in the proposed model.

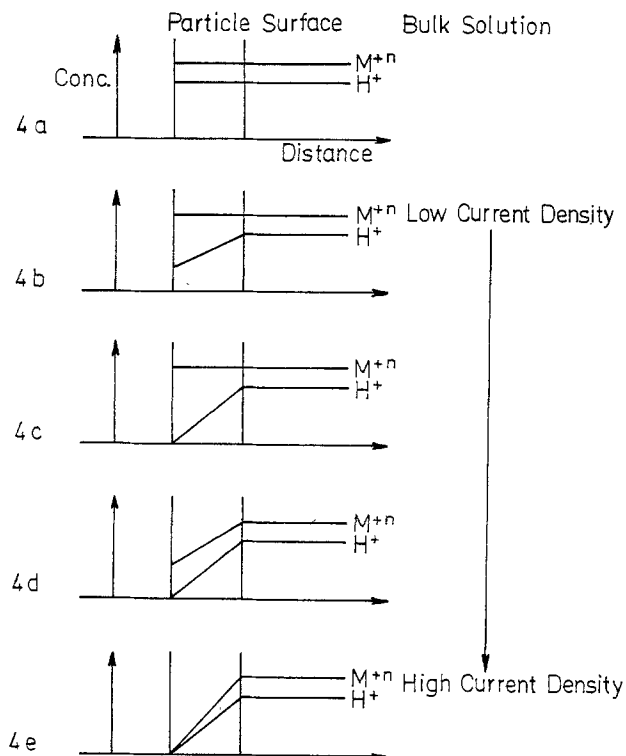


Fig. 4. Concentration profiles of the adsorbed H^+ and Co^{2+} ion on particle at different current densities.

the cathode surface⁷; and (iii) the particles are incorporated irreversibly into the metal matrix by the reduction of some of the adsorbed ions. The Co^{2+} ions in the bulk solution diffuse through the diffusion layer and are deposited on the cathode surface to meet the demands of the reduction process. The partial current is consumed to reduce H^+ ions which diffuse through the diffusion layer from the bulk solution. The adsorbed ions proposed are H^+ and Co^{2+} ions. At steady state, a diffusion layer and concentration profile on the particle surface develop as shown in Fig. 4. When the applied current density is low, the adsorbed H^+ ions on the particle are reduced first. A concentration gradient of H^+ ions on the particle develops as shown in Fig. 4b. Increasing the current density, decreases the concentration of H^+ ion on the particle. The concentration of H^+ ions on the particle approaches zero at limiting case (Fig. 4c). If the current density increases further, both the concentrations of adsorbed H^+ and Co^{2+} ions on the particle are reduced. The concentration gradients of H^+ and Co^{2+} ions develop (Fig. 4d). The concentrations of both H^+ and Co^{2+} ions on the particle surface approach zero (Fig. 4e).

Model development.—The weight percent of the embedded particles is determined by the deposition rate of the metal ions and particles. These two processes are discussed as follows.

Metal deposition.—Although the metal ions may come from the plating solution or the adsorbed ionic cloud, they mainly come from the plating solution. Since the rate-determining step of the reduction of metal ions is the charge transfer reaction, the deposition rate of metal ions can be expressed as

$$V_m = K' \cdot i \cdot \eta^* \cdot (1 - \theta) \quad [2]$$

where V_m is the deposition rate of metal ions, g/min; K' is the constant of the metal deposition rate expression; i is the current density, A/dm²; η^* is the current efficiency; and θ is the strong adsorption coverage.

Particle deposition.—The deposition rate of particles is determined by the reduction of the adsorbed ions on the particles loosely adsorbed. The concentration profiles of H^+

ions and Co^{2+} ions on the particle surface develop as shown in Fig. 4.

(Case 1) When current density is low.—According to Guglielmi's model for the deposition of inert particles,⁷ the deposition rate of particles is equal to the strong adsorption rate of the particle. The particle deposition process can be considered as an electrochemical process with a Tafel expression.⁷ The deposition rate of particles in Guglielmi's model was proposed as

$$V_p = v_0 \exp(B_1\eta) \frac{KC_p}{1 + KC_p} (1 - \theta) \quad [3]$$

where v_0 is a constant for the particle deposition process. It is similar to a constant for an electrochemical process and is a function of concentration of reacting species.¹³ Since the deposition rate of particles is determined by the reduction of the adsorbed ions on the particle, the constant is proportional to the concentration of adsorbed H^+ ions on the particle surface at low current density. The concentration profiles of H^+ ions and Co^{2+} ions are shown in Fig. 4b. The deposition rate of particle can be expressed as

$$V_p = k_1 \exp(B_1\eta) [\text{H}^+]_{x=0} \frac{KC_p}{1 + KC_p} (1 - \theta) \quad [4]$$

where V_p is the deposition rate of particles, g/min; k_1 is the rate constant of particle deposition; $[\text{H}^+]_{x=0}$ is the concentration of adsorbed H^+ ion on the particle surface; B_1 is the constant in the Tafel equation; η is the overpotential, V; K is the equilibrium constant of loose adsorption, and C_p is the particle content in suspension, g/dm³.

Equation 4 is the modification of the equation of strong adsorption in Guglielmi's model.⁷ The concentration of H^+ ion on the particle surface is¹³

$$[\text{H}^+]_{x=0} = \left(1 - \frac{V_p}{V_{p,\text{H}^+}}\right) [\text{H}^+]* \quad [5]$$

where $[\text{H}^+]*$ is the concentration of H^+ ion in the bulk solution; and V_{p,H^+} is the limiting deposition rate of particle due to the reduction of adsorbed H^+ ion on the particle. Substituting Eq. 5 into Eq. 4 yields

$$V_p = k_1 \exp(B_1\eta) \left(1 - \frac{V_p}{V_{p,\text{H}^+}}\right) [\text{H}^+]* \frac{KC_p}{1 + KC_p} (1 - \theta) \quad [6]$$

When particle content in the bulk solution, C_p , is fixed, Eq. 6 can be expressed as

$$\ln\left(\frac{V_p}{1 - V_p/V_{p,\text{H}^+}}\right) = \ln\{k_1[\text{H}^+]* \frac{KC_p}{1 + KC_p} (1 - \theta)\} + B_1\eta \quad [7]$$

(Case 2) When current density is high.—The deposition rate of particles is determined by the reduction of both the adsorbed H^+ ions and Co^{2+} ions on the particle. The concentration profiles of H^+ and Co^{2+} ions on the particle surface are shown in Fig. 4d. The deposition rate of particles can be expressed as

$$V_p = V_{p,\text{H}^+} + k_2 \exp(B_2\eta) [\text{Co}^{2+}]_{x=0} \frac{KC_p}{1 + KC_p} (1 - \theta) \quad [8]$$

where k_2 is the rate constant of particle deposition; $[\text{Co}^{2+}]_{x=0}$ is the concentration of adsorbed Co^{2+} ion on the particle surface; and B_2 is the constant in the Tafel equation.

Similarly, Eq. 8 can be obtained as

$$V_p = V_{p,\text{H}^+} + k_2 \exp(B_2\eta) \left(1 - \frac{V_p - V_{p,\text{H}^+}}{V_{p,\text{Co}^{2+}}}\right) [\text{Co}^{2+}]* \frac{KC_p}{1 + KC_p} (1 - \theta) \quad [9]$$

where $[\text{Co}^{2+}]*$ is the concentration of Co^{2+} ions in the bulk solution; and $V_{p,\text{Co}^{2+}}$ is the limiting deposition rate of particles due to the reduction of adsorbed Co^{2+} ions on the particle.

When particle content in the bulk solution, C_p , is fixed, Eq. 9 can be expressed as

$$\ln\left(\frac{V_p - V_{p,\text{H}^+}}{1 - (V_p - V_{p,\text{H}^+})/V_{p,\text{Co}^{2+}}}\right) = \ln\{k_2[\text{Co}^{2+}]* \frac{KC_p}{1 + KC_p} (1 - \theta)\} + B_2\eta \quad [10]$$

(Case 3) When the reduction of the adsorbed H^+ ions and Co^{2+} ions on the particle are both limited by diffusion.—In this case, the concentration profiles of H^+ ions and Co^{2+} ions are shown in Fig. 4e. The particle deposition rate can be expressed as

$$V_{p,l} = k_3 \frac{KC_p}{1 + KC_p} (1 - \theta) \quad [11]$$

where $V_{p,l}$ is the particle deposition rate in the case of limiting current of the both adsorbed ions; and k_3 is a constant which depends on the concentrations and mass transfer coefficients of H^+ and Co^{2+} ions in the bulk solution. Equation 11 can be rearranged as

$$\frac{1}{V_{p,l}} = k_3 + \frac{k_3}{K} \cdot \frac{1}{C_p} \quad [12]$$

The weight percent of particle in the deposits can be expressed as

$$\beta = \frac{V_p}{V_p + V_m} \quad [13]$$

The model predictions for the weight percent of the embedded particle can be obtained by calculation of Eq. 13.

Results and Discussion

Effects of current density on the weight percent of the embedded particle at different particle content in solution.—The effect of current density on the weight percent of the embedded particle at different suspension concentrations of particle is shown in Fig. 5. At first the weight percent of silicon carbide in the deposits decreased, then increased by increasing the current density at the low current density region. The weight percent of silicon carbide in the deposits has a maximum at the high current density region. The higher the particle content in the suspension solution, the higher the weight percent of particle in the deposits (Fig. 5). The results shown in Fig. 5 are similar to those in Fig. 1. It indicated that Co-SiC and Au- Al_2O_3 codeposition systems have similar behavior which cannot be described by the Guglielmi model.

Effects of current density on the deposition rate of the particle at different particle content in solution.—The deposition rate of particle can be obtained from the product

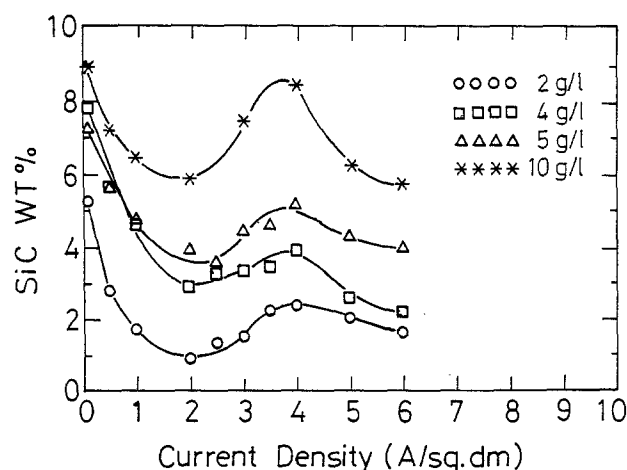


Fig. 5. Effects of current density on the weight percent of particle on deposits at different particle content in solution; operation conditions, pH 4.0; temperature = 30°C; and stirring rate = 400 rpm.

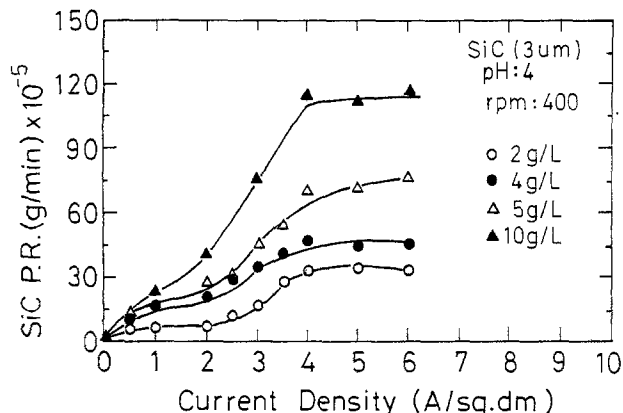


Fig. 6. Effects of current density on the deposition rate of particle at different particle content in solution; operation conditions, pH 4.0; temperature = 30°C; and stirring rate = 400 rpm.

of the total deposition rate and the weight percent of embedded particle. The total deposition rate was determined by microbalance. The effect of current density on the deposition rate of particle at different particle content in solution is shown in Fig. 6. The results imply that the deposition rate of particle increased with increasing the current density and had a limiting deposition rate (V_{p,H^+}) at low current density (0.1-2 A/dm²). When the current density is in the range of 2 to 6 A/dm², the deposition rate of particle increased with increasing the current density again and had another limiting deposition rate ($V_{p,i}$). The more particle content in the solution, the higher the deposition rate of particle. When current density is low, the deposition rate of particle is determined by the reduction of adsorbed H⁺ ion on particles. Since the reduction of the adsorbed H⁺ ion on particles has a limiting current, the deposition rate of particle has a limiting deposition rate (V_{p,H^+}), as shown in Fig. 6. When current density is high, the deposition rate of particle is determined by the reduction of adsorbed H⁺ and Co⁺² ions on the particle. The limiting deposition rate of the particle is determined by the limiting current of the adsorbed H⁺ and Co⁺² ions on the particle at high current density. The qualitative descriptions are consistent with those in the theoretical considerations. The limiting deposition rate contributed by the reduction of adsorbed Co⁺² ion on the particle ($V_{p,Co^{+2}}$) can be obtained as

$$V_{p,Co^{+2}} = V_{p,i} - V_{p,H^+} \quad [14]$$

where $V_{p,i}$ and V_{p,H^+} are the limiting deposition rates at high and low current density, respectively. The values of V_{p,H^+} , $V_{p,i}$ and $V_{p,Co^{+2}}$ at different particle content of solution are shown in Table I. The higher the particle content in solution, the larger the values of V_{p,H^+} , $V_{p,i}$ and $V_{p,Co^{+2}}$.

Effects of effective current density on the deposition rate of cobalt ions at different particle content in solution.—The effective current density can be obtained from the product of current density and current efficiency. The current efficiency is higher than 90% in this codeposition system.

Table I. The limiting deposition rate of particles at different particle content in solution.

C_p (g/cm ³)	V_{p,H^+} (g/min)	$V_{p,i}$ (g/min)	$V_{p,Co^{+2}}$ (g/min)
2	6.0×10^{-5}	32×10^{-5}	26×10^{-5}
4	18×10^{-5}	45×10^{-5}	27×10^{-5}
5	25×10^{-5}	72×10^{-5}	47×10^{-5}
10	—	112×10^{-5}	—

C_p , particle content in solution; V_{p,H^+} , limiting particle deposition rate determined by the reduction of adsorbed H⁺ ion on the particle; $V_{p,Co^{+2}}$, limiting particle deposition rate determined by the reduction of adsorbed Co⁺² ion on the particle; $V_{p,i}$, limiting particle deposition rate.

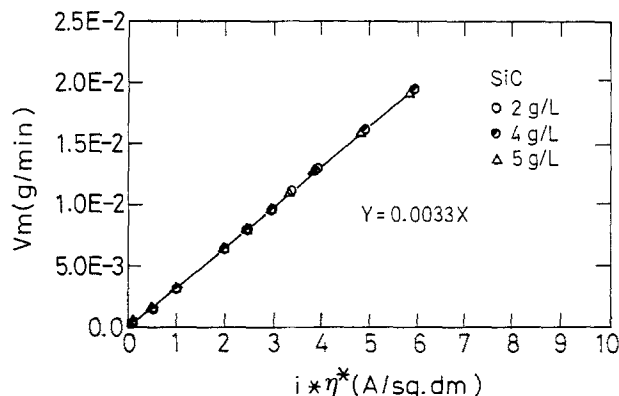


Fig. 7. Effects of effective current density on the deposition rate of cobalt ions at different particle content in solution; operation conditions, pH 4.0; temperature = 30°C; and stirring rate = 400 rpm.

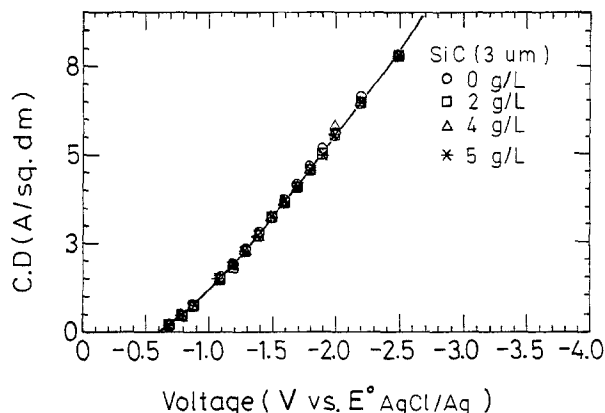


Fig. 8. Effect of particle content in solution on the polarization curves; operation conditions, pH 4.0; temperature = 30°C; and stirring rate = 400 rpm.

The deposition rate of cobalt ions can be obtained from subtracting the deposition rate of particle from the total deposition rate. The effect of effective current density on the deposition rate of cobalt ion at different particle content of solution is shown in Fig. 7. The results indicate that the particle content of solution had no influence on the deposition rate of cobalt ion. The deposition rate of cobalt ion against the effective current density gave a straight line which can be expressed as

$$V_m = 0.0033 \cdot i \cdot \eta^* \quad [15]$$

Comparison of Eq. 15 and Eq. 2, showed that the experimental results were consistent with the theoretical equations. The $K'(1 - \theta)$ can be obtained as 0.0033.

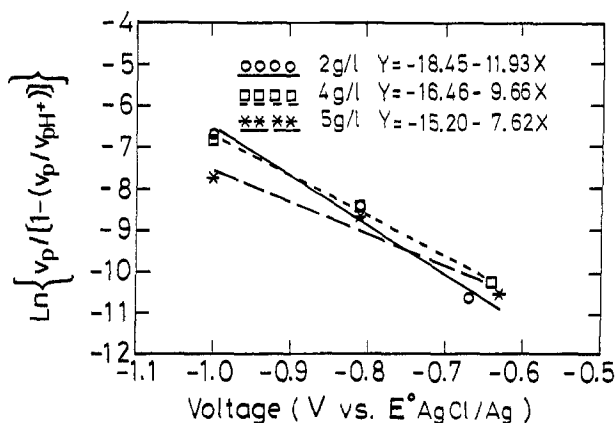


Fig. 9. The plot of $\ln \{V_p / (1 - (V_p/V_{p,H^+}))\}$ against overvoltage at low current density.

Table II. The parameters in the proposed kinetic model for the Co-SiC codeposition system.

C_p	$K'(1 - \theta)$	A_1	B_1	A_2	B_2	$k_3(1 - \theta)$	K
2	0.0033	$e^{-18.45}$	-11.93	$e^{-27.05}$	-12.76	422	0.075
4		$e^{-16.46}$	-9.66	$e^{-22.67}$	-10.20		
5		$e^{-15.20}$	-7.62	$e^{-22.74}$	-9.93		

$A_1, k_1[H^+]*(KC_p/(1 + KC_p))(1 - \theta); A_2, k_2[Co^{+2}]*(KC_p/(1 + KC_p))(1 - \theta).$

Plot of $\ln \{V_p/(1 - V_p/V_{p,H^+})\}$ against overvoltage at low current density.—The overvoltages can be obtained from the polarization curves at different particle content in solution as shown in Fig. 8. It indicates that the particle content in solution has no significant effect on the polarization curve. The plot of $\ln \{V_p/(1 - V_p/V_{p,H^+})\}$ against overvoltage at low current density is shown in Fig. 9. The straight lines at different particle content of solution are obtained. The results correlate well with Eq. 7 in the theoretical consideration. Compare the results in Fig. 9 and Eq. 7, the intercepts and slopes of Eq. 7 can be obtained at different particle content in solution and are shown in Table II.

Plot of $\ln \{(V_p - V_{p,H^+})/(1 - (V_p - V_{p,H^+})/V_{p,Co^{+2}})\}$ against overvoltage at high current density.—The plot of $\ln \{(V_p - V_{p,H^+})/(1 - (V_p - V_{p,H^+})/V_{p,Co^{+2}})\}$ against overvoltage at high current density is shown in Fig. 10. The straight lines at different particle content of solution are obtained. The results are consistent with Eq. 10 in the theoretical consideration. Compare the results in Fig. 10 and Eq. 10, the intercepts and slopes of Eq. 10 can be obtained at different particle content in solution and are shown in Table II.

Plot of $1/V_{p1}$ against $1/C_p$.—The plot of $1/V_{p1}$ against $1/C_p$ is shown in Fig. 11 and given a straight line. The results are

consistent with Eq. 12 in the theoretical consideration. From the intercept and slope of the straight line and Eq. 12, the parameters $k_3(1 - \theta)$ and K can be obtained as shown in Table II.

Comparison of the experimental and theoretical results.—The particle deposition rates can be obtained at different cases. At low current density, Eq. 5 can be rearranged and be given as

$$V_p = D_1/(1 + D_1/V_{p,H^+}) \tag{16}$$

where

$$D_1 = k_1 \exp(B_1\eta)[H^+] * \frac{KC_p}{1 + KC_p} (1 - \theta) \tag{17}$$

At high current density, Eq. 11 can be rearranged as

$$V_p = \left\{ V_{p,H^+} + D_2 \left(1 + \frac{V_{p,H^+}}{V_{p,Co^{+2}}} \right) \right\} / (1 + D_2/V_{p,Co^{+2}}) \tag{18}$$

where

$$D_2 = k_2 \exp(B_2\eta)[Co^{+2}] * \frac{KC_p}{1 + KC_p} (1 - \theta) \tag{19}$$

The model predictions for the weight percent of embedded particles can be calculated by Eq. 13 where V_m and V_p can be obtained from Eq. 15-18. The parameters in Eq. 15-18 can be obtained from Table II. Comparison of the experimental and theoretical model results is shown in Fig. 12 which indicates that the experimental results correlate well with the theoretical model results. The proposed model can describe the mechanism of codeposition of Co-SiC system well.

Conclusion

The mechanism of codeposition of silicon carbide with the electrolytic cobalt was proposed. The experimental results can be described qualitatively and quantitatively by the proposed model. The particle deposition rates are determined by the reduction of the adsorbed H^+ and Co^{+2} ions on the particle. At low current density, the particle deposition rates are determined mainly by the reduction of adsorbed

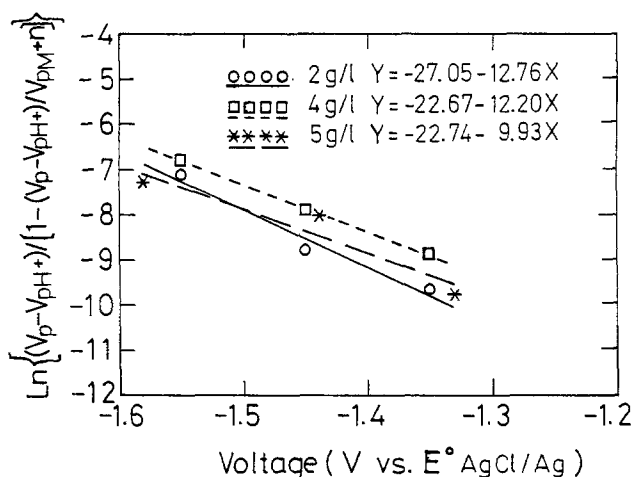


Fig. 10. The plot of $\ln \{(V_p - V_{p,H^+})/(1 - (V_p - V_{p,H^+})/V_{p,Co^{+2}})\}$ against overvoltage at high current density.

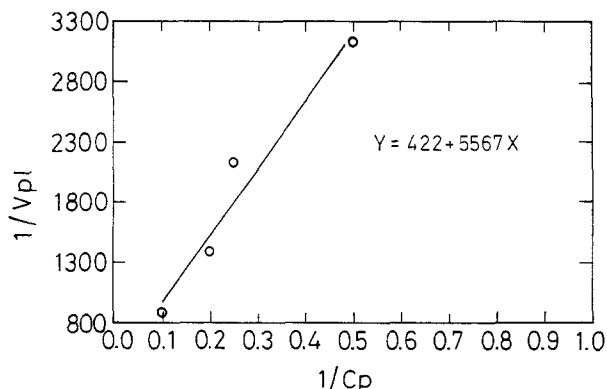


Fig. 11. The plot of $1/V_{p1}$ against $1/C_p$.

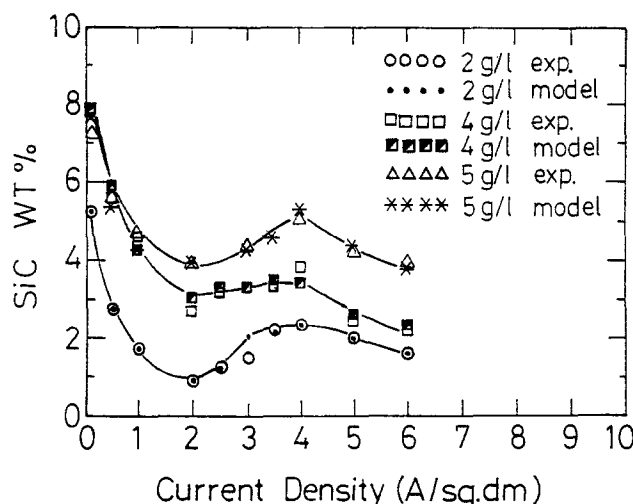


Fig. 12. Comparison of the experimental results and theoretical model calculations.

H⁺ ion on the particle. At high current density, the reduction of both ions are important to the deposition rate of the particle. The parameters in the theoretical model were obtained by comparison with the experimental results. The experimental results were predicted well with the model simulation.

Acknowledgment

The support of the National Science Council (NSC 79-0410-E011-02) and National Taiwan Institute of Technology of the Republic of China are acknowledged.

Manuscript submitted Jan. 14, 1992; revised manuscript received Jan. 4, 1993.

The National Science Council of the Republic of China assisted in meeting the publication costs of this article.

LIST OF SYMBOLS

A	constant in the Tafel equation relating to the metal deposition
A ₁	constant in the Tafel equation relating to the particle deposition at low current density
A ₂	constant in the Tafel equation relating to the particle deposition at high current density
B	constant in the Tafel equation relating to the particle deposition
B ₁	constant in the Tafel equation relating to the particle deposition at low current density
B ₂	constant in the Tafel equation relating to the particle deposition at high current density
[Co ²⁺] _{x=0}	concentration of adsorbed Co ²⁺ ion on the particle surface
[Co ²⁺]*	concentration of Co ²⁺ ion in bulk solution
C _p	particle concentration in solution, g/dm ³
d	density of the deposited metal, g/dm ³
D ₁	defined in Eq. 16
D ₂	defined in Eq. 18
F	Faraday constant
[H ⁺] _{x=0}	concentration of adsorbed H ⁺ ion on the particle surface
[H ⁺]*	concentration of H ⁺ ion in bulk solution
k ₁	rate constant of particle deposition expression
k ₂	rate constant of particle deposition expression
k ₃	constant in Eq. 11
K	equilibrium constant of loose adsorption

K'	constant of metal deposition rate expression
i	applied current density, A/dm ²
i ₀	constant in the Tafel equation relating to metal deposition
n	no. of electron transfer
v ₀	constant in the Tafel equation relating to particle deposition
V _m	deposition rate of metal ions, g/min
V _p	deposition rate of particles, g/min
V _{p,H⁺}	limiting deposition rate due to the reduction of adsorbed H ⁺ ion on the particle
V _{p,Co²⁺}	limiting deposition rate due to the reduction of adsorbed Co ²⁺ ion on the particle
V _{p,l}	particle deposition rate in the case of limiting current of the adsorbed ions
W	atomic weight, g/mol

Greek

η	overpotential, V
α	volume fraction of particle in the deposits
β	weight percent of the embedded particle
η*	current efficiency
θ	strong adsorption coverage

REFERENCES

1. C. Buelens, J. P. Celis, and J. R. Roos, *J. Appl. Electrochem.*, **13**, 541 (1983).
2. M. Ghouse and E. G. Ramachandran, *Met. Finish.*, June, 85 (1981).
3. M. Ruimi and R. Martinou, *ibid.*, July, 7 (1989).
4. M. Thoma, *Plating Surf. Finish.*, Sept., 51 (1984).
5. J. Zahavi and J. Hazan, *ibid.*, Feb., 57 (1983).
6. E. S. Chen and F. K. Sautter, *ibid.*, Oct., 28 (1976).
7. M. Gulielmi, *This Journal*, **119**, 1009 (1972).
8. J. P. Celis and J. R. Roos, *ibid.*, **124**, 1508 (1977).
9. N. Masuko and K. Mushiaki, *J. Met. Finish. Soc. Jpn.*, **28**, 534 (1982).
10. M. K. Totlani and S. N. Athavale, *J. Electrochem. Soc. India*, **31**, 119 (1982).
11. A. M. J. Kariapper and J. Foster, *Trans. Inst. Met. Finish.*, **52**, 87 (1974).
12. J. P. Celis, J. R. Roos, and C. Buelens, *This Journal*, **134**, 1402 (1987).
13. A. J. Bard and L. R. Faulkner, *Electrochemical Methods—Fundamentals and Applications*, pp. 27-29, 109, John Wiley & Sons, Inc., New York (1980).

Thermodynamics of Adsorption of Brighteners on Polarized Nickel from Watts Bath Solution

T. Mimani and S. M. Mayanna

Department of Chemistry, Central College, Bangalore University, Bangalore 560 001, India

ABSTRACT

The adsorption of coumarin, nitrocoumarin, and p-toluene sulfonamide on nickel from Watts bath solution has been studied using a polarization technique. The exchange current densities (i_0) with and without additives were evaluated using a Tafel relation. The addition agents inhibited the deposition process. Surface coverages calculated from the i_0 values were fit into the Langmuir adsorption isotherm. Thermodynamic parameters (ΔG_a° , ΔH_a° , and ΔS_a°) for the adsorption of the addition agents have been evaluated using the Bockris-Swinkles adsorption isotherm. The values of ΔG_a° are negative indicating the strong interaction and reactive inhibition of the deposition process by these additives. The electrodeposition interaction is discussed from the viewpoint of the adsorption of the additive molecules on the metal solution interface.

In recent years, electroplating technology has gained considerable importance because of its widespread applications in metal finishing industries. Trace levels of additives are used in the electroplating baths to impart tailor-made properties to the electrodeposits. These additives act as inhibitors in the electrodeposition process. However, they participate so decisively¹ that understanding the inhibition action requires a knowledge of the adsorption of the inhibitor at the electrode solution interface.² Adsorption of

inhibitors during metallic corrosion³⁻⁵ and electrodeposition⁶ have been studied earlier.

Nickel coatings find extensive applications in the automotive, electronics, and telecommunication industries. Nickel is typically electroplated from a Watts bath containing aromatic sulfones or sulfonamides and coumarin as effective brighteners. The behavior of coumarin at a rotating nickel disk electrode⁷ and at the interface between mercury and the electrolyte solution⁸ has been studied. The extent of